Article

Activation of Methane on NiO Nanoparticles with Different Morphologies

Ruth L. Martins and Martin Schmal[*,#]

*Federal University of Rio de Janeiro, NUCAT-PEQ-COPPE, Bl G-128, Centro de Tecnologia,
21945-970 Rio de Janeiro-RJ, Brazil*

Superfícies nanoestruturadas podem ser definidas como substratos tendo como principal característica dimensões na faixa de 1-100 nm. O recente interesse nestes sistemas é baseado no fato de que novas e interessantes propriedade (catalíticas, magnéticas, ferroelétricas, mecânicas, óticas e eletrônicas) são desenvolvidas como resultado da redução da dimensão destes substratos. Neste trabalho descreve-se a decomposição catalítica do metano em hidrogênio e nanofilamentos de carbono em catalisadores não suportados de Ni preparados por metodologias distintas. Catalisador de Ni suportado em zircônia foi usado para comparação dos resultados. Para os catalisadores não suportados, observou-se forte dependência da atividade do catalisador com o tamanho da partícula do óxido precursor e sua morfologia. Apesar de todos terem apresentado dimensões na faixa de nanopartículas, somente os preparados usando etileno glicol, NiEG, e rota hidrotérmica, NiHT, exibiram a mesma performance que o catalisador suportado (atividade e estabilidade), 25NiZ. O catalisador sintetizado em presença de dimetilglioxima, NiDMG, foi o menos ativo e desativou com o tempo em operação.

Nanostructured surfaces can be defined as substrates in which the typical features have dimensions in the range of 1-100 nm. The recent focus of interest in these systems is based on the fact that interesting novel properties (catalytic, magnetic, ferroelectric, mechanical, optical and electronic) are developed as a result of the dimension reductions of these substrates. This paper describes the catalytic methane decomposition into hydrogen and carbon nanofilaments on unsupported Ni catalysts prepared from different methodologies, with controlled particle size and morphologies. Ni catalyst supported on zirconia was also used for performance comparison. For the unsupported catalysts, it was observed strong dependency of catalyst activities with particle size of nickel oxide precursors and their morphologies. Although all of them presented crystallite sizes with nanometric dimensions, only those prepared with ethylene glycol, NiEG, and by hydrothermal condition, NiHT, exhibited the same performance as the supported catalyst (activity and stability), 25NiZ. Catalyst synthesized in the presence of dimethylglyoxime, NiDMG, was less active and deactivated with time on stream.

Keywords: NiO, nanoparticles, H_2 production, carbon nanofilaments

Introduction

There are many new challenges ahead in the field of heterogeneous catalysis in terms of the chemical process and reactions to be promoted by the use of nano catalysts. As an example, the conversion of methane, which is usually performed by different direct or indirectly routes, require specific catalysts. Non oxidative methane process is relevant for investigating the different possibilities of methane activation and posterior interaction between the molecules or intermediates and the surface of the catalyst and thus, for understanding the reaction mechanisms governing the formation of C–C bonding, the reaction condition influencing the formation of these ligands, as well as, the product distribution, which are of fundamental interest, not only for the non-oxidative coupling but also on processes related to the methane transformation.

Martins *et al.*[1] reported the role of different supports (silica, alumina and zirconia) on the non-oxidative conversion of methane on Pt loaded catalysts, with or without the presence of MoO_3. Moya *et al.*[2] studied the non-oxidative methane coupling on nanostructured

*e-mail: schmal@peq.coppe.ufrj.br
[#]Present adress: Dept. Chem. Eng., University of São Paulo, 05424-970 São Paulo-SP, Brazil

supported palladium catalysts and Antje Ota *et al.*[3] studied the particle size effect in methane activation over supported palladium nanoparticles. Moya *et al.*[4] studied the monodispersed and nanostructrured Ni/SiO$_2$ catalyst for the non-oxidative methane activation.

Also, direct cracking of methane on supported Ni catalyst were reported in the literature.[5-7]

$$CH_4 \rightarrow C + 2H_2, \ \Delta H_{298°} = 75.6 \ kJ \ mol^{-1} \qquad (1)$$

This process is moderately endothermic, with little gain in energy needed *per* mol of H$_2$ production and the reaction is thermodynamically favored at higher temperatures. The H$_2$/CH$_4$ is low during methane cracking with carbon structure formation. Direct cracking forms nanofilament carbons with graphite planes as precursor. On supported nickel catalysts, hydrocarbons are decomposed at the interface gas-metal followed by dissolution and carbon diffusion through the metal particles. These carbons then precipitate at the interface, dragging out the metallic particle of the support with the formation of carbon filaments, as observed by Aiello *et al.*[8] for the Ni/SiO$_2$ and Alberton *et al.*[9] for the Ni/Al$_2$O$_3$ catalysts. Methane cracking for hydrogen production was studied over Ni/Ni alloy catalysts supported on pure or WO$_3$/MoO$_{3-}$ modified zirconias by Martins *et al.*.[10] On unsupported Ni nanoparticles there are formation of carbon nanotubes.

Metallic catalysts, in the catalysis concept, are usually prepared by the deposition of small nanometer-sized particles (< 20 nm) of an active phase, a metal, finely dispersed on a cheaper high-surface-area support, commonly a porous oxide. The dispersion is used mainly to improve the surface-to-volume ratio of the active phase. Additionally, this practice also leads to a better distribution of reaction heat, better poison resistance, and improve catalyst life by preventing metal sintering. Supported catalysts are prepared by impregnation of the porous solid with a precursor metal salt followed by oxidation and reduction pretreatments. However, that practice leads to the formation of nanoparticles with a wide range of sizes and shapes displaying a distribution of surface sites capable of promoting many different reactions. No molecular control on the nature of the active sites is expected, and only limited control on the selectivity of reactions can be achieved. Controlling the size of the nanoparticles used for catalysis can lead to huge changes in catalytic behavior. The importance of nanoparticles and nanostructure to the performance of catalysts has stimulated wide efforts to develop methods for their synthesis and characterization, making this area of study an integral part of nanoscience.[11] Fortunately, metal nanoparticles can now be made with quite narrow size distributions by using,

beside others, colloidal[12] or dendrimer[13] based chemistry. The morphology of these materials depends on the syntheses conditions, and has been described by different authors as nanotowers, nanocone, nanobottle, nanoflowers, nanoarrows, nanorod, nanowires and so on. The challenge is to disperse the colloidal nanoparticles on high-surface area supports and to activate them without losing the original size and shape distribution. As a matter of fact, the control of the morphology of the nanoparticles, perhaps, seems to be more important than monitoring the performance of catalysts by controlling the size of the nanoparticles of the active phase. It has been known that some catalytic processes are structure sensitive, meaning that their activity or selectivity changes significantly with the method used for the catalyst preparation.

In this work, we present methane activation on Ni nanoparticles with different morphologies synthesized by different methods for the methane activation and characterized before and after activation of methane.

Experimental

Preparation of catalysts

Ni catalysts with 25 wt.% of NiO were prepared by incipient wetness impregnation of Ni(NO$_3$)$_2$.6H$_2$O, using as ZrO$_2$ precursor the Zr(OH)$_4$ (MEL Chemical). Usually zirconia, obtained by calcination of Zr(OH)$_4$ at 923 K, involves two phases: stable monoclinic zirconia (M) and metastable tetragonal zirconia (T). The zirconia obtained by calcination of pure Zr(OH)$_4$ at 923 K for 3 h is mostly monoclinic, while Ni modified zirconias (where Ni content is equal or greater than 20 wt.%) are predominantly tetragonal in structure.[10] After drying at 373 K for 24 h, the catalyst was calcined in the presence of synthetic air at 923 K for 3 h, at a ramping rate of 1 K min^{-1}.

The NiO with controlled crystallite sizes were prepared by three different methods.

(i) Precipitation of nickel hydroxide with sodium carbonate precursor salts dissolved in ethylene glycol (EG) (NiEG) according to Li *et al.:*[14] Ni(NO$_3$)$_2$.6H$_2$O was dissolved in ethylene glycol (0.05 mol in 150 mL of EG), heated gradually at 393 K under stirring and kept at this temperature for 30 min, followed by drop wise addition of a solution of 500 mL of 0.2 mol L^{-1} of Na$_2$CO$_3$, aged for 1 h at 393 K, filtered, washed with distilled-deionized water and then dried at 373 K for 16 h. The resulting sample was calcined at 673 K for 4 h flowing synthetic air at 50 mL min^{-1}.

(ii) Precipitation of nickel dimethylglyoxyme as precursor (NiDMG) according to Ni *et al.*:[15] 3 g of Ni(NO$_3$)$_2$.6H$_2$O was dissolved in 650 mL of distilled-

deionized water. A solution of 334 mL of ethanol containing 1% of dimethylglyoxyme was added dropwise to the solution with the formation of a red precursor of Ni(DMG)$_2$. After centrifugation and washing with distilled-deionized water, the precipitated solid was dried at 373 K for 16 h and calcined at 673 K for 4 h under atmospheric air and heating rate of 3 K min^{-1}.

(iii) NiO was obtained after hydrotreatment and calcination of β-Ni(OH)$_2$ precursor (NiHT) according to Zhu *et al.*:[16] about 1 mmol of Ni(CH$_3$COO)$_2$.4H$_2$O was dissolved in 5 mL distilled-deionized water followed by addition of 15 mL ethanol and 5 mL of CO(NH$_2$)$_2$, under strong stirring. Then, adding 2 mL of NH$_4$OH (35% v/v) drop by drop, resulting a strong blue solution with the formation of a complex [Ni (NH$_3$)$_6^{2+}$]. This solution was transferred to an autoclave, coated by Teflon and heated in a furnace at 120 °C for 12 h. After cooling, the resulted precipitate was centrifuged and washed several times with distilled-deionized water, dried at 50 °C for 8 h, forming the (β-Ni(OH)$_2$) precipitate. NiO was formed after calcination at 673 K for 4 h and a heating rate of 3 K min^{-1}.

Characterizations

The X-ray powder diffraction measurements were performed in a Rigaku Miniflex diffractometer operated at 30 kV and 40 mA, using the graphite monochromated Cu Kα radiation. The diffractograms were recorded over 2θ values ranging from 10 to 90°, with a scanning rate of 2 s step^{-1} and 0.02 step sizes.

Sample images were recorded in a field emission gun scanning electron microscope (FEG-SEM) (FEI Company) model QUANTA 400, equipped with an energy dispersive X-ray spectroscopy (EDS) system without treatment. The samples were first dispersed in isopropyl alcohol, using ultrasonic bath for 10 min, then a small amount of this solution was dropped on a copper grid and dried before analysis.

Catalytic tests

Temperature programmed surface reaction (TPSR) experiments were carried out, by using pure methane at 50 cm^3 min^{-1}, varying the temperature from 298 to 773 K, at a heating rate of 10 K min^{-1}. The masses of catalyst used were 25 mg for the unsupported and 100 mg for the supported catalysts, respectively. TPSR experiments were performed in a Micromeritics TPD/TPR 2900 equipment coupled to a Balzers quadrupole mass spectrometer as detector. The gases used were CH$_4$ (99.95% purity), He (99.995 purity).

Activity tests were conducted at atmospheric pressure in a Pyrex micro reactor of fixed bed using 100 mg of the supported and 25 mg of the unsupported Ni catalysts, respectively. Output gases were analyzed in a gas chromatograph coupled online brand Varian, model CP-3800 GC, equipped with column CP Poraplot Q, operating in isothermal condition. He was used as carrier gas. The products were analyzed by flame ionization detector (FID) and thermal conductivity detector (TCD). Before reaction, the catalysts were pretreated with pure CH$_4$, at 30 cm^3 min^{-1}, 773 K, and heating rate of 10 K min^{-1}.

Results

Temperature programmed surface reaction (TPSR) and XRD analyses before and after reaction

The adsorption and decomposition mechanism of methane on metallic surfaces is an exothermic activation process of dissociative and homolytic in nature. The kinetics of CH$_4$ adsorption on metallic surfaces has been studied in the literature by TPSR on different supported metals, films and crystallites. However, there is little about the methane decomposition on unsupported nanosized metallic crystals. Therefore, we prepared the nanosized crystallites by different methods, which were tested and characterized before and after the reaction decomposition and after exposure of the catalyst to methane for 5 h.

The supported 25NiZ and unsupported NiEG catalysts

Temperature programmed surface reaction results for the supported 25NiZ catalyst are presented in Figure 1a, showing the methane (*m/z* 15), hydrogen (*m/z* 2) and water (*m/z* 18) profiles with increasing temperature up to 773 K and at a heating rate of 10 K min^{-1}. Figure 1b shows the profiles of the unsupported NiEG sample.

The behavior of these samples is quite different. For the supported 25NiZ sample, the water profile (*m/z* 18) increases initially with time on stream but after reaching a maximum peak it decreases, indicating firstly methane decomposition and simultaneously H$_2$ (*m/z* 2) consumption, which can be attributed to the reduction of NiO to metallic sites and water formation. In fact, methane is highly decomposed initially, decreasing then with time at lower conversion, indicating thus the partial deactivation of the catalyst, due to the carbon deposition. On the other hand, the unsupported NiEG sample showed constant profiles with time on stream after initial activation, including for water (*m/z* 18), suggesting a slower process of NiO reduction during the reaction. No longer had
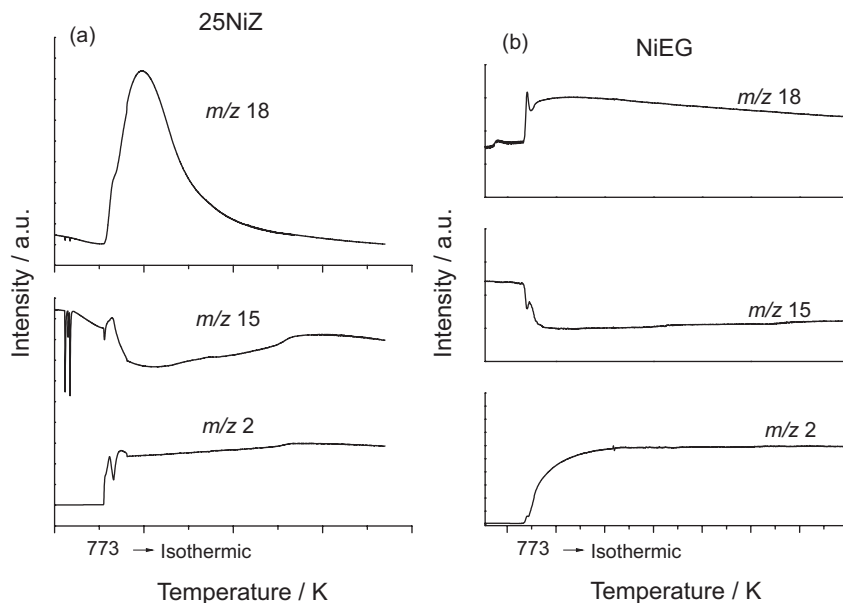
Figure 1. Temperature programmed surface reaction profiles (TPSR) of 25NiZ (a) and NiEG (b) catalysts.

deactivation occurred, but only decomposition of methane at higher conversions.

In fact, the diffractograms of the supported 25NiZ catalyst before and after reaction, which are presented in Figure 2A, evidence firstly the presence of a tetragonal phase of zirconia and before reaction only the nickel oxide. However, after reaction, it presents only metallic Ni^0 cubic phase, as shown in the diffraction peaks at 44.5° (111), 51.8° (200) and 76.4° (220). Besides, there are diffraction peaks at 26° (002) and 42° (101), which are assigned to the carbon phase as graphite structure.

Figure 2B displays the diffractograms of the unsupported NiEG sample before and after reaction. Before the reaction, exhibits diffraction peaks at 37.26° (111), 43.28° (200), 62.88° (220), 75.38° (311) and 79.75° (222), which are assigned to NiO cubic phase. After reaction, exhibits diffraction peaks at 44.5°, 51.8° and 76.4°, which are attributed to the metallic Ni^0, besides the peaks at 26° (002) and 42° (101), corresponding to a graphite structure.

The unsupported NiDMG sample

Figure 3A displays the mass spectra profiles of H_2O, CH_4 and H_2 of the NiDMG sample. Different from the previous NiEG sample, the NiDMG catalyst lost activity, since the H_2 evolution and methane consumption decreased with time on stream, after initial decomposition of methane and activation of NiO into metallic Ni^0.

Indeed, Figure 3B shows the diffractograms of the unsupported NiDMG catalyst before and after reaction at 773 K for 5 h. Before the reaction, there are diffraction

lines attributed to NiO cubic phase, beside the diffraction lines assigned to the Ni^0 metallic crystalline phase.
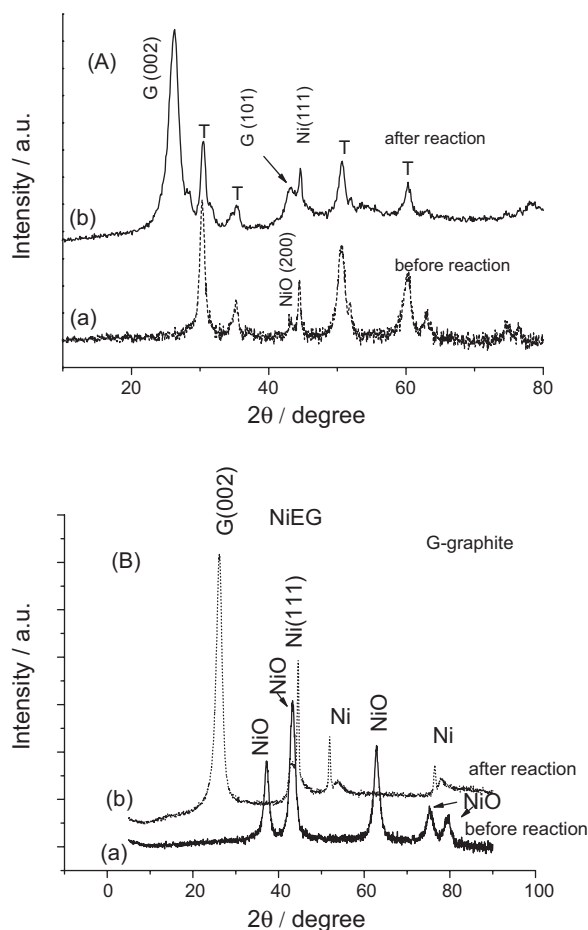
Figure 2. XRD of 25NiZ catalyst (A) before (a) and after (b) reaction; XRD of the NiEG catalyst (B) before (a) and after (b) reaction: G: graphite; T: tetragonal zirconia.

However, after the reaction, it shows only diffraction lines corresponding to the Ni[0] metallic phase and of the graphite structure. However, when compared to the previous NiEG, these graphite diffraction lines are less intense.
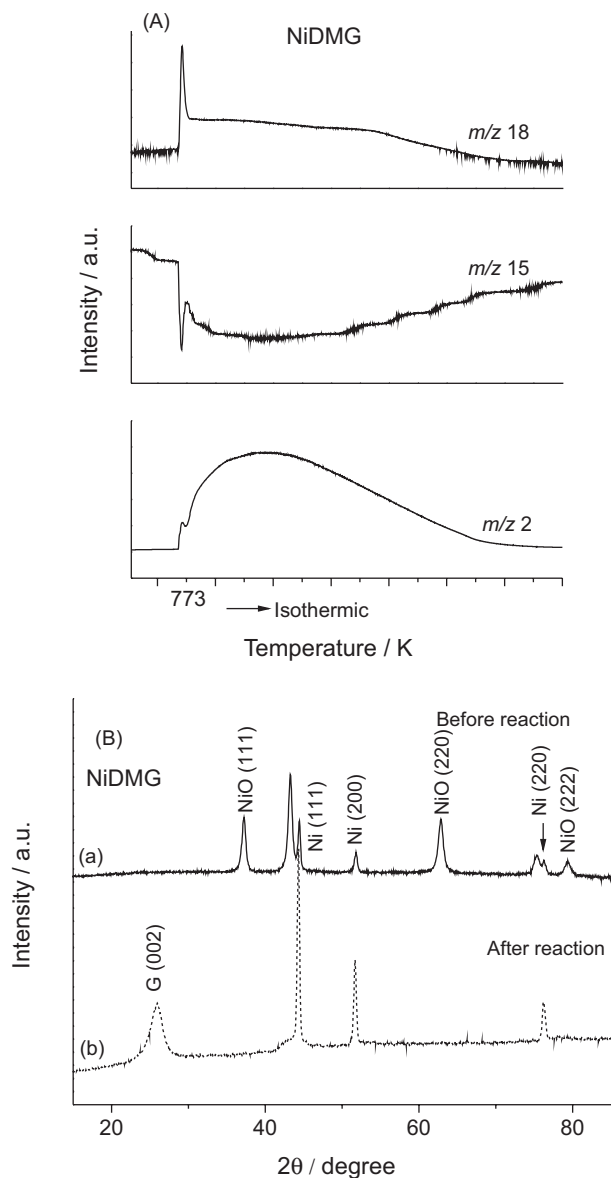
Figure 3. Temperature programmed surface reaction profiles (TPSR) of 25NiDMG (A); (B) XRD diffraction of the NiDMG catalyst before (a) and after (b) reaction decomposition at 773 K.

The hydrotermal precursor (NiHT)

The unsupported NiHT was obtained after hydrotreatment and calcination of β-Ni(OH)$_2$ precursor.[16] Figure 4A displays the profiles of methane decomposition on the NiHT with increasing temperature. Like the NiEG sample, the profiles are very similar during the reaction. After an initial activation of Ni species by methane, which was done during time on stream, as evidenced by the

profile of water formation, methane is decomposed, with the formation H$_2$ at a constant level.

Figure 4B displays the diffratograms of the NiHT before and after exposition to methane at 773 K by 5 h. Before reaction, the diffraction pattern shows the lines corresponding to the NiO cubic phase. After treatment, only refraction lines corresponding to metallic Ni[0] phase and graphite were observed.
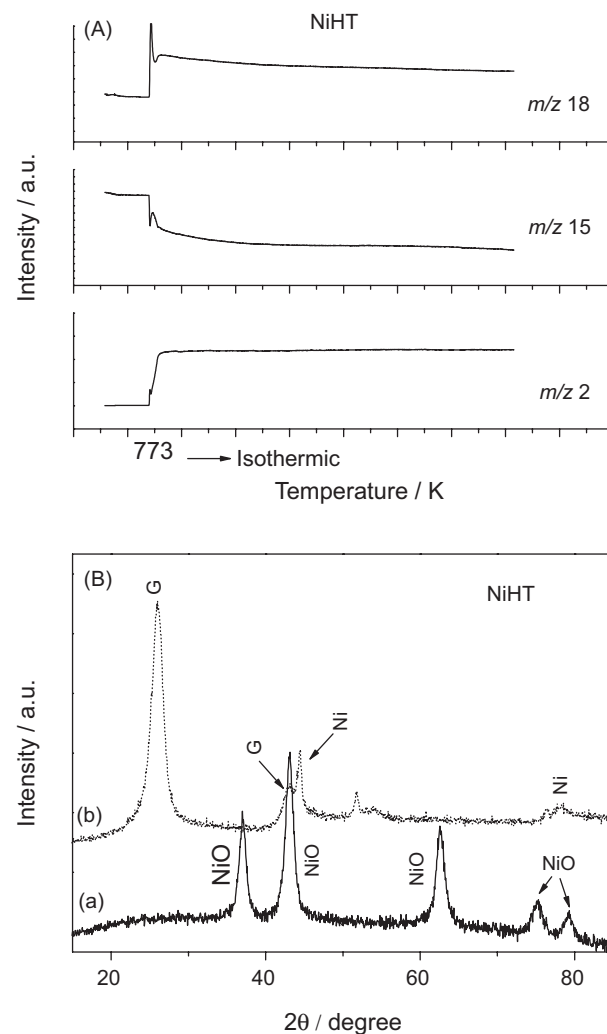
Figure 4. Profiles during CH$_4$ decomposition with increasing temperature of NiHT (A); XRD of the NiHT sample (B): before (a) and after (b) CH$_4$ decomposition at 773K. G: graphite.

Scanning electronic microscopy (SEM-FEG)

Figure 5 displays the scanning electronic microscopic analyses. Figure 5a shows a nanoflower like type morphology in tridimensional form of NiO on the NiEG sample before the reaction. This morphology was originally observed on the hydroxide before calcination and seems to be very stable after thermal pretreatment; thus, removing water did not damage the structure of the precursor.

The structure did not collapse or fracture, which can be attributed to the excellent contact between nanoparticles with high orientation degree.[14]

Figure 5b shows SEM images of NiO after calcination of the NiDMG precursor, indicating the presence of bidimensional rods, which suggests made up of small particles that gather forming rods. By removing the organic molecule (DMG) during heating, the arrangement of the structure of the precursor NiDMG was not affected, and according to Gui *et al.*,[17] heating probably supplies energy to maintain the NiO nanoparticles highly oriented in the structure.
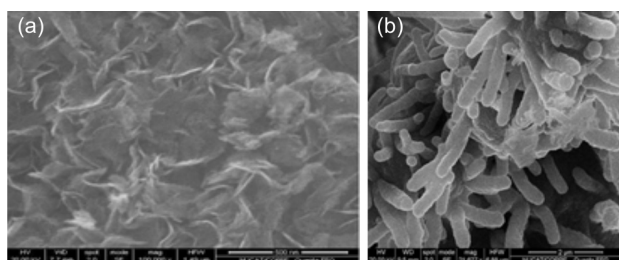
Figure 5. SEM images of the NiEG sample (a) in oxide form: 100000×; SEM images of the NiDMG sample (b) in oxide form, 20000×.

SEM images of the NiHT sample are displayed in Figure 6. The images are similar to the images of the NiEG sample, exhibiting nanosheets arranged with bends and hollow structure forming nanoflowers. However,
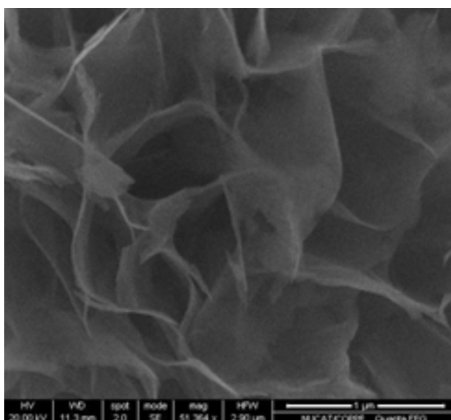
Figure 6. SEM images of the NiHT sample.
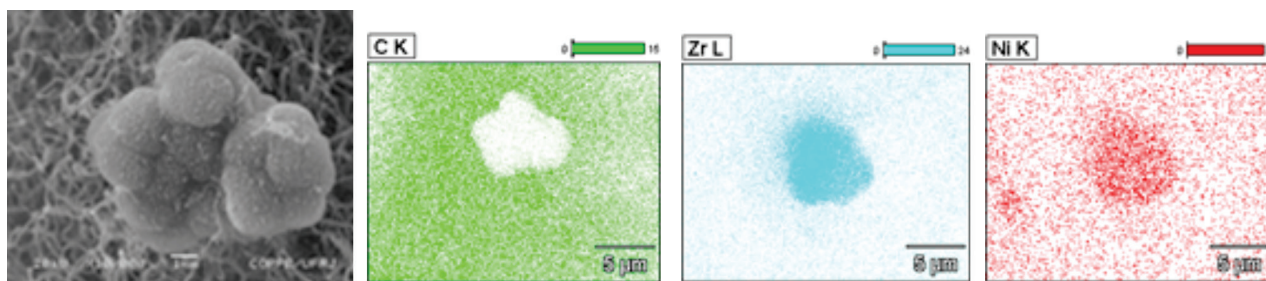
comparing the images, it seems that the NiHT sample presents structures, which are less compacted. Zhu *et al.*[16] claims that urea and ammonia influence the formation of tridimensional structure during the preparation of the hydroxide precursor. The absence of urea results in a flaked structure and the absence of ammonia results in a structure in the form of combs.

Figure 7 displays the SEM images with the EDS analysis of C, Zr and Ni of 25NiZ catalyst after 5 h of methane exposition at 773 K. As observed by Aiello,[8] on supported nickel catalysts, methane is decomposed at the interface gas-metal followed by dissolution and carbon diffusion through the metal particles. These carbons then precipitate at the interface dragging out the metallic particle of the support with the formation of carbon nanofilaments with metal particles at the tip. The EDS images show clearly the grain of zirconia free from carbon particles with Ni particles well dispersed on it as well as on carbon nanofilaments.

Figure 8 displays the SEM images of NiEG after 5 h of methane exposition at 773 K. On unsupported Ni nanoparticles (NiEG, NiDMG and NiHT), there is formation of carbon nanofilaments, which acted as living supports taking the catalyst particles away and preventing them from sintering with adjacent particles. By this way, the metal particles are located at the tip of nanotubes.

Activity tests

Activity tests were conducted at atmospheric pressure in a Pyrex micro reactor of fixed bed using 100 mg of the supported and 25 mg of the unsupported Ni catalysts at 773 K. Catalysts were pretreated with pure CH_4 at 30 cm^3 min^{-1} and 773 K, and heating rate of 10 K min^{-1}.

Figure 9 displays the results of the conversion of methane at 773 K for all catalysts. The unsupported NiEG, NiHT and the supported Ni catalysts (25NiZ) presented similar behavior and conversions around 9% with time on stream. However, the NiDMG catalyst presented much lower conversion, although the crystal sizes in nano size dimensions as the previous samples.

Figure 7. SEM image of 25NiZ with EDS analysis of C, Zr and Ni after 5 h of methane exposition at 773K.
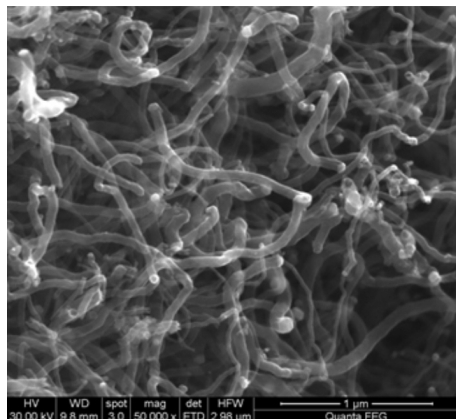
Figure 8. SEM image of NiEG after 5 h of methane exposition at 773 K.
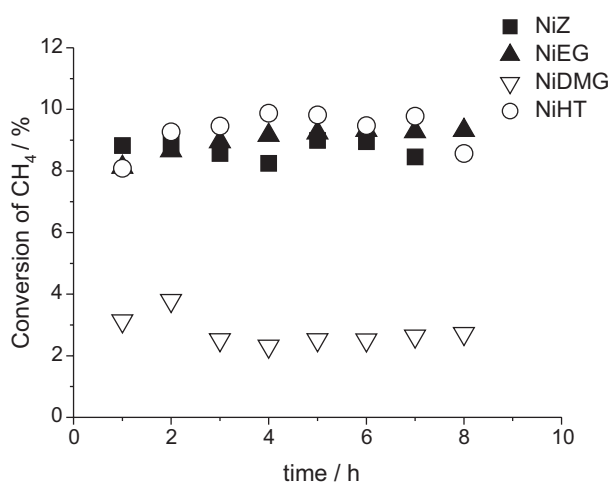
Figure 9. Conversion of methane on supported 25NiZ, and unsupported NiEG, NiDMG and NiHT catalysts.

Discussion

In *et al.*[18] studied comparatively chemisorption and methane conversion on metallic crystallite surfaces calculating the dissociation energy of C–H bonds of methane and showed that the main dissociated species is CH_3, because it has the highest energetic barrier to split the bonding, as observed for the reaction $CH_3 \rightarrow CH_2 + H^*$ over all surfaces. The higher the adsorption strength, the higher is the energy necessary to move surface species that migrate over the surface to meet other fragments for reacting. They concluded that ethylene should be formed through dehydrogenation of ethane and not by coupling of methane. Ciobica *et al.*[19] calculated that on Ru (1120), the most stable species is CH_2^* and that the intermediates CH_x $(1 < x < 3)$ are more stable when adsorbed on bridged sites, while C species are preferentially adsorbed on top sites.

As described in our previous paper,[9] the first step of the homologation reaction is the adsorption of methane, followed by the hydrogenation step. During the adsorption of methane, there are different surface carbon adspecies,

which can be hydrogenated. The H_2 evolution resulted from the association of hydrogen atoms provided from dissociative chemisorption of methane, as indicated by equations 2 and 3:

$$CH_4 + 2^* \rightarrow CH_{3ads} + H_{ads} \tag{2}$$
$$H_{ads} + H_{ads} \rightarrow H_2 + 2^*, \text{ where } ^* \text{ represents } Ni^0 \text{ sites} \tag{3}$$
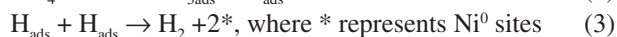
However, methane conversion increased besides water consumption during the reaction. These results suggest decomposition of methane (equation 2) besides methane reforming (equation 5).

$$CH_4 \leftrightarrow C + 2H_2 \qquad \Delta H^o_{298\,K} = 76 \text{ kJ mol}^{-1} \tag{4}$$
$$CH_4 + H_2O \rightarrow CO + 3H_2 \quad \Delta H^o_{298\,K} = 206.2 \text{ kJ mol}^{-1} \tag{5}$$

However, CO was not detected, which suggests that shift reaction may occur (equation 6), due to the presence of water, during the activation process, beside the CO decomposition, according to Bourduard (equation 7) and the dry reforming (equation 8).

$$CO + H_2O \rightarrow CO_2 + H_2 \qquad \Delta H^o_{298\,K} = -41.2 \text{ kJ mol}^{-1} \tag{6}$$
$$2CO \rightarrow C + CO_2 \qquad \Delta H^o_{298\,K} = -172.0 \text{ kJ mol}^{-1} \tag{7}$$
$$CH_4 + CO_2 \rightarrow 2CO + 2H_2 \quad \Delta H^o_{298\,K} = 247 \text{ kJ mol}^{-1} \tag{8}$$

X-ray results

The commonly accepted model of methane decomposition and carbon growth on nickel catalysts consists of three stages:[20,21] (*i*) methane molecules adsorb dissociatively on active surface Ni (100) and Ni (110) planes of the catalysts, which may exist as small aggregated nickel crystals, (*ii*) carbon diffuses into the bulk of the nickel crystallite and filaments would rapidly grow on the Ni (111) face of the crystallite due to the coincidental symmetry between the Ni (111) and the graphite (002) plane, (*iii*) nickel crystallites will be dragged out on the tip of the growing carbon filament. This will also prevent small crystallites contacting with neighboring particles or sintering into bigger ones.

To maintain the continuous growth of carbon nanofilaments or nanotubes, the balance between the methane decomposition rate, carbon diffusion rate and the precipitation rate can be achieved by using appropriate catalyst particle sizes. The disequilibrium occurs when the dissociation rate is much faster than the carbon diffusion rate and subsequently carbon layers will be formed on the active surfaces of the catalysts, resulting in the so-called deactivation process.[22] The initial carbon nanofilaments act as transporting agent and support to take individual particles

away, and prevent sintering with adjacent particles of the catalyst, as displayed in Figures 7 and 8 for 25NiZ and NiEG catalysts. Other factors influencing the feasibility of carbon filament formation include the particle size and the surface area. Smaller particle sizes and larger surface areas (more porous structure) increase the probability for methane molecules to reach the active surface and to draw the nickel crystallites away and be supported on the tip of carbon nanofibers, thus preventing them from sintering into bigger crystals. It was interesting to note that the active Ni particles during the reaction were usually on the tip of one carbon nanofiber only. However, Wang et al.,[23] upon closer inspection of deactivated unsupported Ni catalyst, found that two Ni particles collided and coalesced together with two carbon nanofibers connecting them. In fact, the micrographs of the totally deactivated Ni catalysts suggest that the collisions between two Ni catalyst particles or between Ni particles and carbon nanofibers might also be a reason contributing to catalyst deactivation.

The crystallite sizes of the nano structured catalyst before the reaction were calculated according to Sherrer's equation and the results are presented in Table 1. As seen, the crystallite sizes changed from 6 nm to 27 nm, and depend on the preparation method. The supported 25NiZ catalyst presented bigger crystallites (27 nm), while the unsupported NiEG the lowest value (6 nm). These values are in the range of nanosized crystallites.

Tabel 1. Crystallite sizes of NiO of different precursors before reaction, reaction rates of the methane conversion and carbon formed during time on stream

Catalyst	Crystal size / nm	Rate × 10^5 / [mols $(g_{NiO}.s)^{-1}$]	Carbon / g
NiEG	6	7.14	0.935
NiDMG	15	2.68	0.13
NiHT	8.4	7.14	0.745
5NiZ	27	8.04	0.835

In our previous paper,[17] we prepared nickel nanoparticles for the non-oxidative methane activation. A nickel acetate solution was impregnated on silica support and then reduced with $NaBH_4$ (NiB/SiO_2) exhibiting only metallic Ni^0 particles of the order of 15 nm. Part of this solid was then oxidized under mild conditions, where Ni ions were re-structured and redistributed as a $Ni-Ox/SiO_2$ oxide solid that, after reduction with hydrogen, favored the formation of smaller Ni^0 particles of the order of 3.5 nm. Comparing the results, one can conclude that crystallite sizes of the unsupported NiEG, which was prepared by precipitation of nickel hydroxide with sodium carbonate precursor salts

dissolved in ethylene glycol[14] (NiEG), are comparable to the method prepared by impregnation of a nickel acetate[17] in contrast to the 25NiZ supported sample, which presented crystallite sizes 4 times bigger than the unsupported NiEG.

Activity

The reaction rates are presented in Table 1 for different catalysts. The rates of the NiO on the NiEG and NiHT precursors are similar and approximately equal to the reaction rate of the supported 25NiZ sample [8.04×10^{-5} mols $(g_{NiO}.s)^{-1}$], used as reference, but three times more active than the NiDMG sample [2.68×10^{-5} mols $(g_{NiO}.s)^{-1}$]. In fact, the activity seems to depend on the morphology. In particular, it suggests that the nanoflower like type NiEG exposes nanosized NiO crystallites for the methane decomposition or dissociation, which increases the activity. On the other hand, the nanorod shape crystallites, like NiDMG precursor, are less active and probably less stable.

The results indicate that these catalysts are active for the dissociation or decomposition of methane and for the formation of carbon nanospecies species of high reactivity at the surface. Quantitatively, there are significant differences between the different samples, the supported 25NiZ and the unsupported NiEG, NiHT and NiDMG samples, where the first three exhibited three times more adsorption capacity than the last one. Indeed, the metal oxide crystal sizes of the NiEG and NiHT are approximately 2 times lower than of NiDMG precursor, with exception of the supported 25NiZ catalyst (Table 1). In fact, Table 1 presents the carbon formation of the different samples and shows that the amount of carbon formation is related to the activity of the different NiO morphologies. In our previous study,[4] we observed that although the particle sizes of NiB/SiO_2 and $Ni-Ox/SiO_2$ differ by a factor of 5, the activity at 773 K or adsorption capacity of the $Ni-Ox/SiO_2$ catalyst was three times more active than NiB/SiO_2. The adsorption capacity is attributed to the metallic nanostructured particles. Therefore, the results suggest that the structure of the metal oxide and the morphology in particular, affect the methane dissociation.

Koerts[24] observed and classified the surface carbon species as C_α, C_β and C_γ. The most reactive is the carbide C_α type, followed by the less active C_β carbon, which is amorphous. The C_γ or graphitic carbon is the less active. According to authors, the C_α carbon species are formed on low surface coverages. Winslow et al.[25] and Duncan[26] indicated that methane is initially dissociated in C_α carbon adsorbed species, which can be transformed immediately to C_β, both phases in dynamic equilibrium. However, the C_β carbon species can be slowly transformed by aging

into irreversible C_γ species, at rates depending on the temperature and structure of the catalyst.

The dissociative adsorption of methane on Ni catalysts has been studied by different authors, showing that the estimated value of the energetic barrier of methane dissociation on Ni (100) crystal surface faces were 0.28 eV[27] and 0.54 eV[28] and for Ni (111) crystal surface 0.77eV.[29] Theoretical calculations indicated energetic barriers in the range of 0.69 ± 0.04 eV for methane dissociation on Ni (100) surfaces.[30] In fact, calculations[31] by density functional theory (DFT) estimated energy value of 0.60 eV on Ni (100) surface; however, the presence of oxygen inhibits the methane dissociation, which is attributed to the decreasing interaction between CH_3 and H atoms with the substrate. Therefore, to increase the exposition at the surface of the Ni (100) face, it is necessary to change their morphology. In fact, it suggests that nanostructures of nanoflowers like type may address the specific topology.

Conclusions

The NiO catalysts prepared using different methods for controlling the particle sizes with different organic precursors and $Ni(NO_3)_2.6H_2O$ as source of Ni, were active for methane activation with H_2 and carbon nanotubes production. The initial carbon nanotubes acted as transporting agents and supports to take individual catalyst particles away and prevent them from sintering with adjacent particles. The results of this work indicate that there is a strong dependence of crystallite sizes and, in particular of the morphology, with the activation of methane and their stability. Crystallites of the order of magnitude of nanostructure favor the dissociation of methane and inhibit aggregation and formation of bigger particles that conducts to deactivation. The NiO of the NiEG and NiHT precursor presented crystallite sizes of the order of 6 and 8 nm, respectively, while the NiO of NiDMG precursor presented crystallite sizes of the order of 15 nm.

The activities of the NiO on the NiEG and NiHT precursors are similar and approximately equal to the activity of the 25NiZ supported sample and three times more active than the NiDMG precursor. As a matter of fact, it seems that the morphology and crystallite sizes of NiDMG catalyst leads methane dissociation rate much faster than the carbon diffusion rate and subsequently carbon layers of graphite will be formed on the active surfaces of the catalysts, resulting in the so-called deactivation process. Carbon nanofibers can only be produced when the balance between methane dissociation rate and carbon diffusion rate is maintained. In fact, the activity and the nano structured crystallites sizes depend on the morphology, which suggests that the nanoflower like type beside achieves the proper carbon diffusion rate and the precipitation rate, increases the exposing Ni (100) crystal surface for the methane decomposition or dissociation. Also, its structure stability can be attributed to the excellent contact between nanoparticles with high orientation degree.

Acknowledgments

References

1. Martins, R. L.; Baldanza, M. A. S.; Souza, M. M. V. M.; Schmal, M.; *Appl. Catal., A* **2007**, *318*, 207.

2. Moya, S. F.; Martins, R. L.; Ota, A.; Kunkes, E. L.; Behrens, M.; Schmal, M.; *Appl. Catal., A* **2012**, *411-412*, 105.

3. Ota, A.; Kunkes, E. L.; Krohnert, J.; Schmal, M.; Behrens, M.; *Appl. Catal., A* **2013**, *452*, 203.

4. Moya, S. F.; Martins, R. L.; Schmal, M.; *Appl. Catal., A* **2011**, *396*, 159.

5. Muradov, N. Z.; *Energy Fuels* **1998**, *12*, 41.

6. Poirier, M. G.; Sapundzhiev, C.; *Int. J. Hydrogen Energy* **1997**, *22*, 429.

7. Choudhary, T. V.; Goodman, D. W.; *Catal. Lett.* **1999**, *59*, 93.

8. Aiello, R.; Fiscus, J. E.; zur Loye, H-C.; Amiridis, M. D.; *Appl. Catal., A* **2000**, *192*, 227.

9. Alberton, A. L.; Souza, M. M. V. M.; Schmal, M.; *Appl. Catal., B* **2011**, *103(3-4)*, 326.

10. Martins, R. L.; Baldanza, M. A. S.; Alberton, A. L.; Vasconcelos, S. M.; Schmal, M.; *Appl. Catal., B* **2011**, *103*, 326.

11. Bell, A. T.; *Science* **2003**, *299*, 1688.

12. Grass, M. E.; Yue, Y.; Habas, S. E.; Rioux, R. M.; Teall, C. I.; Yang, P.; Somorjai, G. A.; *J. Phys. Chem. C* **2008**, *112*, 4797.

13. Albiter, M. A.; Zaera, F.; *Appl. Catal., A* **2011**, *391*, 386.

14. Li, Y.; Zhang, B.; Xie, X.; Liu, J.; Xu, Y.; Shen, W.; *J. Catal.* **2006**, *238*, 412.

15. Ni, X.; Zhao, Q.; Zhou, F.; Zheng, H.; Cheng, J.; Li, B.; *J. Cryst. Growth* **2006**, *289*, 299.

16. Zhu, L. P.; Liao, G. H.; Yang, Y.; Xiao, H. M.; Wang, J. F.; Fu, S. Y.; *Nanoscale Res. Lett.* **2009**, *4*, 550.

17. Gui, Z.; Liv, J.; Wang, Z.; Song, L.; Hu, Y.; Fan, W.; Chen, D.; *J. Phys. Chem. B* **2005**, *109*, 1113.

18. In, Y. Z.; Sun, J.; Yi, J.; Lin, J. D.; Chen, H. B.; Liao, D. W.; *J. Mol. Struct.* **2002**, *587*, 63.

19. Ciobica, I. M.; van Santen, R. A.; *J. Phys. Chem. B* **2002**, *106*, 6200.

20. Li, Y. D.; Li, D. X.; Wang, G. W.; *Catal. Today* **2011**, *162*, 1.

21. Dupuis, A. C.; *Prog. Mater. Sci.* **2005**, *50*, 929.

22. Yang, R. T.; Chen, J. P.; *J. Catal.* **1989**, *115*, 52.

23. Wang, H. Y.; Lua, A. C.; *J. Phys. Chem.* **2012**, *116*, 26765.

24. Koerts, T.; Deelen, M. J. A.; van Santen, R. A.; *J. Catal.* **1992**, *138*, 101.

25. Winslow, P.; Bell, A. T.; *J. Catal.* **1985**, *94*, 385.

26. Duncan, T. M.; Winslow, P.; Bell, A. T.; *J. Catal.* **1985**, *93*, 1.

27. Beebe Jr, T. P.; Goodman, D. W.; Kay, B. D.; Yates, J. T.; *J. Chem. Phys.* **1987**, *87*, 2305.

28. Chorkendorff, I.; Alstrup, I.; Ullmann, S.; *Surf. Sci.* **1990**, *227*, 291.

29. Egeberg, R. C.; Ullmann, S.; Astrup, I.; Mullins, C. B.; Chorkendorff, I.; *Surf. Sci.* **2002**, *497*, 183.

30. Swang, O.; Faegri Jr., K.; Gropen, O.; Wahlgren, U.; Siegbahn, P.; *Chem. Phys.* **1991**, *156*, 379.

31. Xing, B.; Pang, X-Y.; Wang, G-C.; Shang, Z-F.; *J. Mol. Catal. A: Chem.* **2010**, *315*, 187.